Catalysis Today 444 (2025) 114997

Contents lists available at ScienceDirect

Catalysis Today

journal homepage: www.elsevier.com/locate/cattod

Biodiesel photoelectrocatalytic synthesis employing α-Fe_2O_3 film decorated with Pt nanoparticles as photoanode

Wagner N. Soares [a], Antonio G.R. Costa [b], Rejane M.P. Silva [b], Sidney G. Lima [a], Tiago P. Braga [c], Isolda Costa [d], Geraldo E. Luz Jr [a,b], Reginaldo S. Santos [a,b,*]

[a] Department of Chemistry, Federal University of Piauí - UFPI, Campus Ministro Petrônio Portella, Ininga, Teresina, PI 64049-550, Brazil
[b] PPGQ-GrEEnTec, State University of Piauí - UESPI, 2231 João Cabral Street, P.O. Box 381, Teresina, PI 64002-150, Brazil
[c] Chemistry Institute, Federal University of Rio Grande do Norte - Laboratório de Peneiras Moleculares (LABPEMOL), Natal 59078-970, Brazil
[d] Institute for Energy and Nuclear Research - IPEN/CNEN, University City, São Paulo, SP 05508-000, Brazil

ARTICLE INFO

Keywords:
Renewable energy
Hematite electrodes
Platinum nanoparticles
Electrochemical Synthesis

ABSTRACT

In this work, photoelectrochemical route for biodiesel production using an electrochemical cell configured with platinum and α-Fe_2O_3 modified with Pt nanoparticles as electrodes was investigated. XRD patterns registered for film prepared by modified hydrothermal method revealed a trigonal structure of the hematite (α-Fe_2O_3) phase. The α-Fe_2O_3 film surface was decorated by metallic Pt nanoparticles (Pt^{NP}) in order to reduce the charge recombination and improve the photocatalytic efficiency. The band gap energy (E_{BG}) of the α-Fe_2O_3 and Pt^{NP}/α-Fe_2O_3 films was estimated by UV-Vis spectroscopy at approximately 2.1 eV. Electrochemical measurements showed that the oxide is an n-type semiconductor adequate to be used as a photoanode in biodiesel synthesis. Under polarization conditions, the electrochemical cell changed the pH from 7 to 14 when the system was polarized at 5.0 V. In the synthesis of biodiesel by esterification reaction, oleic acid, 300 μL of 0.1 mol L^{-1} aqueous KCl solution and methanol were used as precursor reagents. The reaction was carried out free of strong base, such as KOH or NaOH, as a supporting electrolyte. In this route, the reduction of the water molecule occurred on the cathode, with the formation of hydroxyl (OH^-) species, methoxy, and consequently fatty acid methyl esters (FAMEs). Thermogravimetric analysis (TGA) and Gas chromatography coupled to mass spectrometry (CG-MS) were performed to evaluate the catalysis products. GC-MS analyzes show that the reaction has a yield of about 7 % with the formation of FAMEs, such as methyl 9-octadecenoate, methyl hexadecanoate and methyl hexadecanoate.

1. Introduction

The gradual reduction of oil reserves associated with its dependence as the main fuel source has motivated studies to discover alternative energy sources. Diesel is still one of the most used fuels in combustion engines. In this context, research has been carried out in recent decades to find alternative energy sources capable of reducing our dependence on oil and its derivatives [1,2]. In this context, biodiesel, which can be obtained from renewable precursor sources such as oils, fats, and alcohol (ethanol), has emerged as a more suitable candidate [3]. Therefore, it becomes an ecological, biodegradable fuel and, compared to diesel, has a favorable carbon balance for reducing greenhouse gases [4,5].

Biodiesel can be obtained by microemulsions, thermal cracking, transesterification, and esterification methods [6–8]. Among them, the most used are transesterification and esterification. In transesterification, the biodiesel is obtained by a catalytic reaction between triglycerides and a short-chain alcohol; while in esterification the reaction is between a fatty acid and an alcohol. Both processes can be carried out by homogeneous or heterogeneous catalysis, although alkaline homogeneous catalysis is the most used on the industrial scale [9,10]. This biodiesel synthesis method can promote soap formation, decreasing the biodiesel production reaction efficiency and making it difficult to separate the biofuel from the glycerol, a transesterification reaction byproduct.

In 2009 Guan et al.[11]. presented a pioneering study on the preparation of biodiesel by electrolysis methodology. In that study, the authors presented the electrochemical route as an alternative to avoid the saponification reaction during the oil conversion into biodiesel. In

* Correspondence to: Department of Chemistry-PPGQ, State University of Piauí - UESPI, Campus Poeta Torquato Neto, Pirajá, Teresina, PI 64002-150, Brazil.
E-mail address: rsantos.uespi@gmail.com (R.S. Santos).

https://doi.org/10.1016/j.cattod.2024.114997
Received 15 April 2024; Received in revised form 10 July 2024; Accepted 15 August 2024
Available online 15 August 2024

general, through the electrochemical route, the esterification or transesterification reaction is initiated with OH^- species formed on the cathode from the electrolysis of water in the reaction system. The water reduction on the cathode electrode must occur as presented in Eq. 1:

$$2H_2O+2e^-\rightarrow H_2+2OH^- \quad (1)$$

In addition to water molecules, in the biodiesel electrochemical synthesis, the reaction system is usually composed of alcohol, oil, or fatty, co-solvent to improve the reactant miscibility, and salt as a supporting electrolyte. The supporting electrolyte has the function of improving conductivity and reducing the Ohmic potential of the reaction medium [12]. Some studies have used strong bases such as NaOH or KOH as supporting electrolytes, probably because the reaction presented in Eq. 1 is favored for alkaline media [11,13–15].

The electrochemical method for biodiesel synthesis can be considered a clean route and capable of avoiding the saponification reaction. Furthermore, as the electrodes are responsible for the OH^- species formation, biodiesel washing after the synthesis stage to catalyst removal from the rational system is unnecessary. If the reaction is esterification, the product formed will also be free of glycerol formed during the transesterification reaction [16].

Previous studies developed by our research group showed that oxygen evolution reactions (OER) occurred at relatively low potentials on hematite (α-Fe_2O_3) electrodes [17]. This property suggests that hematite crystals favor the dissociation of H_2O molecules and, therefore, may be suitable as photoelectrode for the preparation of biodiesel via the electrochemical route. In addition, previous studies show that platinum nanoparticles (Pt^{NP}) on the electrodes act as co-catalysts, favoring photocatalytic reactions [18,19]. α-Fe_2O_3 is a semiconductor oxide that has properties that allow its use in solar energy conversion [20,21]. Due to its good electrochemical stability in alkaline aqueous solution and short gap band gap energy (2.0–2.2 eV), hematite has been widely used as a photoanode in many photocatalytic processes [22]. This material is abundant in the earth's crust and can absorb visible light regions. However, α-Fe_2O_3 displays some disadvantages, such as low-speed surface reactions, small diffusion coefficient of photoexcited electrons, and charge recombination due to defects present in its crystalline structure [20,22]. These disadvantages can be overcome or minimized using metallic nanoparticles anchored on the oxide surface, which act as co-catalysts. Among nanoparticles investigated, platinum (Pt^{NP}) stands out [23,24].

There are reports of biodiesel preparation using semiconductor oxides as a catalyst material, which act as heterogeneous acid or alkaline catalysts, depending on their composition. For example, Safaripour, et al. [25]. synthesized biodiesel using a magnetic graphene oxide decorated with titanium oxide and silver nanoparticles. In this study, it was demonstrated that the nanoparticles improve the catalytic capacity of the heterogeneous catalyst. Also, Guo et al.[26]. prepared biodiesel from water cooking oil by photocatalytic method on CuO/ZnO nanoparticles. In both works, semiconductor oxides were used as catalysts dispersed in the reaction medium.

The additional concentration of OH^- due to the presence of strong base and co-solvent in the reaction system should favor the transesterification reaction for biodiesel synthesis via electrochemical route. However, these additional reagents can make the process less environmentally friendly and more expensive. Based on that, this study aims to investigate biodiesel synthesis by photoelectrocatalysis using hematite film (α-Fe_2O_3) modified with platinum nanoparticles as photoelectrodes. The preparation of biodiesel from the esterification of oleic acid was carried out using an electrochemical cell without co-solvent and any alkaline compound, such as KOH or NaOH. Furthermore, the α-Fe_2O_3 film was characterized structurally, optically, morphologically and photoelectrochemically.

2. Experimental

2.1. Preparation and modification of α-Fe_2O_3 films with Pt^0 nanoparticles

α-Fe_2O_3 film was prepared based on the purpose-built materials (PBM) method, according to the condition described previously by our research group [17]. Initially, a conductive transparent substrate formed by Fluorine doped tin oxide (FTO) layered on glass (FTO-glass) was cut into dimensions of 1.0×4.5 cm^2. The FTO-glass substrates were previously washed before the film deposition, employing an ultrasound system in three consecutive steps. In these steps, neutral soap, deionized water and isopropyl alcohol were used, consecutively.

The hematite films were synthesized from 20 mL of a 0.15 mol L^{-1} solution of iron(III) chloride hexahydrate and 20 mL of 0.076 mol L^{-1} sodium sulfate, which were placed in a glass autoclave, adapted with the support of Teflon, as presented in Fig. 1. Then the FTO-glass was partially immersed into the iron oxide precursor solution.

To prepare α-Fe_2O_3 film by the PBM method, the autoclave was placed in an oven and heated at a temperature of 120°C for 1 h in order to promote a formation process of a compound named iron(III) oxide hydroxide (β-FeOOH) directly under the FTO-glass substrate. During the reaction, a yellow-brown substance film was obtained. After that, the films were washed in deionized water using ultrasound for 5 min. The samples were dried at room temperature and subjected to thermal treatment at 500 °C for 2 h, in a muffle furnace in an oxidizing atmosphere. The thermal treatment changed the color of the sample for a red-brown film, characteristic of the hematite phase (α-Fe_2O_3), the process described is represented by Fig. 1.

The surface modification of α-Fe_2O_3 films with platinum (Pt^0) nanoparticles (NPs) was performed by the photoreduction method, according to the methodology previously investigated by our research group[19]. In this method, Pt^{NPs} were obtained from 1.0×10^{-3} mol L^{-1} aqueous solutions of hexachloroplatinic acid hexahydrate ($H_2PtCl_6.6\,H_2O$). The α-Fe_2O_3 films were immersed in Pt precursor solutions in a 10 mL beaker for 10 s. After that, the films were placed in a closed box configured with three lamps (STAR LUX, 20 W), at approximately 40 cm from the irradiation source. The films were left under UV irradiation for 5 min. Then, the films were washed with deionized water to remove excess unreduced platinum. Fig. 1 presents a complete scheme of the synthesis and surface modification process of the hematite film.

2.2. Structural, optical, and morphological characterization of the films

X-ray diffraction (XRD) patterns of the films were obtained using a Shimadzu Lab XRD-6000 model diffractometer operating with CuKα radiation ($\lambda = 0.15406$ nm) at 40 kV and 30 mA, 2θ diffraction incident angle ranging from 10° to 70°, angle range of 0.02° and scanning rate of 1°/min. Diffraction patterns were compared with crystalline information data for inorganic compounds obtained from the Inorganic Crystal Structure Database (ICSD). The optical properties of the films were investigated by spectroscopy measurements in the visible UV-Vis region in the transmittance spectrum, using a Shimadzu spectrophotometer (Model UV-2600) and FTO-glass as a reference. The band gap energies (E_{bg}) of films were obtained by the Tauc method, from UV-Vis curves registered in transmittance mode [27,28]. In this method, the E_{bg} is obtained from extrapolation of the linear part of the graphs of $[\alpha h\upsilon]^{0.5}$ as a function of the incident photon energy ($h\upsilon$), considering the indirect transition for these materials. A field-emission scanning electron microscope (FEG-SEM) Quanta FEG 250 was utilized to investigate the film surface morphology.

2.3. Photoelectrochemical characterization of the films

The photoelectrochemical measurements were carried out using a three-electrode system, the working electrode being hematite films

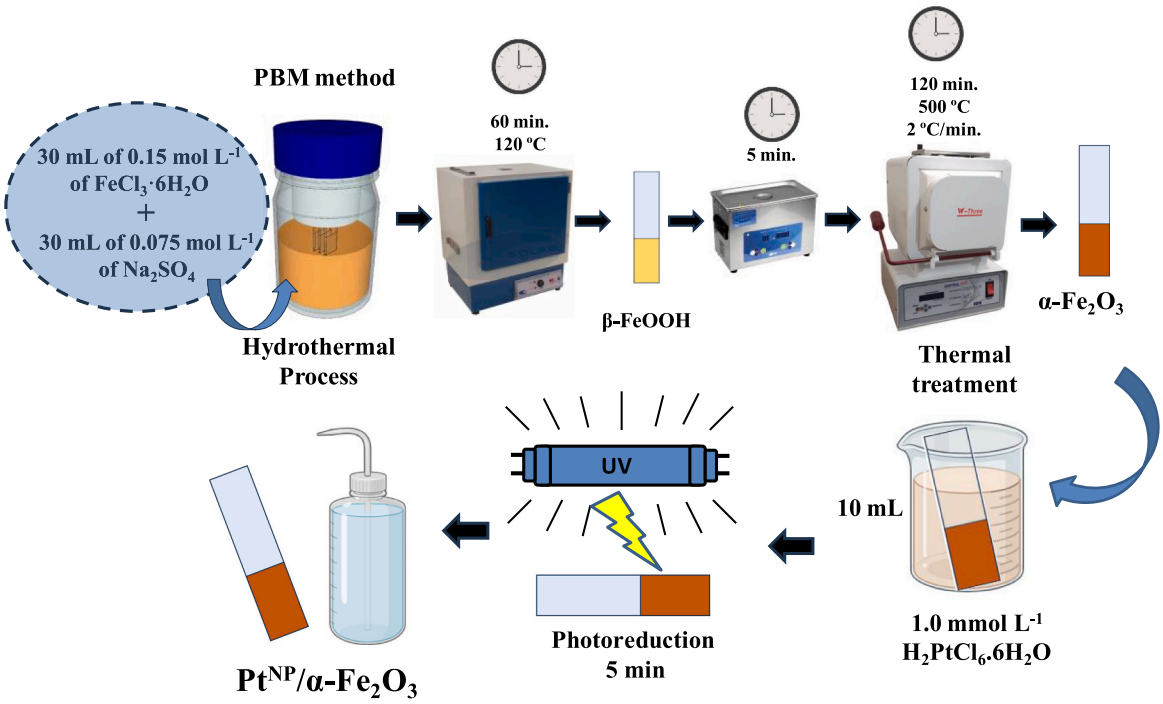

Fig. 1. Scheme of the synthesis of hematite films. In order: Autoclave adapted with Teflon support, film after hydrothermal (β-FeOOH), and film after calcination (α-Fe_2O_3), respectively.

(geometric area of 1.5 cm^2), the counter electrode being a Pt wire and the reference electrode, Ag/AgCl (3.0 mol L^{-1} KCl) placed in a Luggin capillary. The photoelectrochemical analyses were carried out in a Potentiostat/Galvanostat (Autolab PGSTAT 302-N from Metrohm), controlled by NOVA 1.7 Software. The studies were registered in the absence of light (condition named dark) and under polychromatic irradiation with a metallic vapor lamp (Osram HQI-TS EXCELLENCE NDL–150 W). Linear sweep voltammograms (LSV) were recorded with the scan rate of 2 mV/s under manual light interruption (0.2 Hz) to obtain flat band potential (E_{fb}) using the Burtler-Gartner model [28,29]. Chronoamperometry curves were recorded under dark conditions and irradiation with a polarized electrode at a constant potential of 0.8 V (*vs* Ag/AgCl) with a chopper every 100 s under irradiation.

2.4. *Biodiesel synthesis by photoelectrocatalysis*

For the synthesis of biodiesel, an electrochemical cell configured with two electrodes was used, as schematized in Fig. 2. To apply

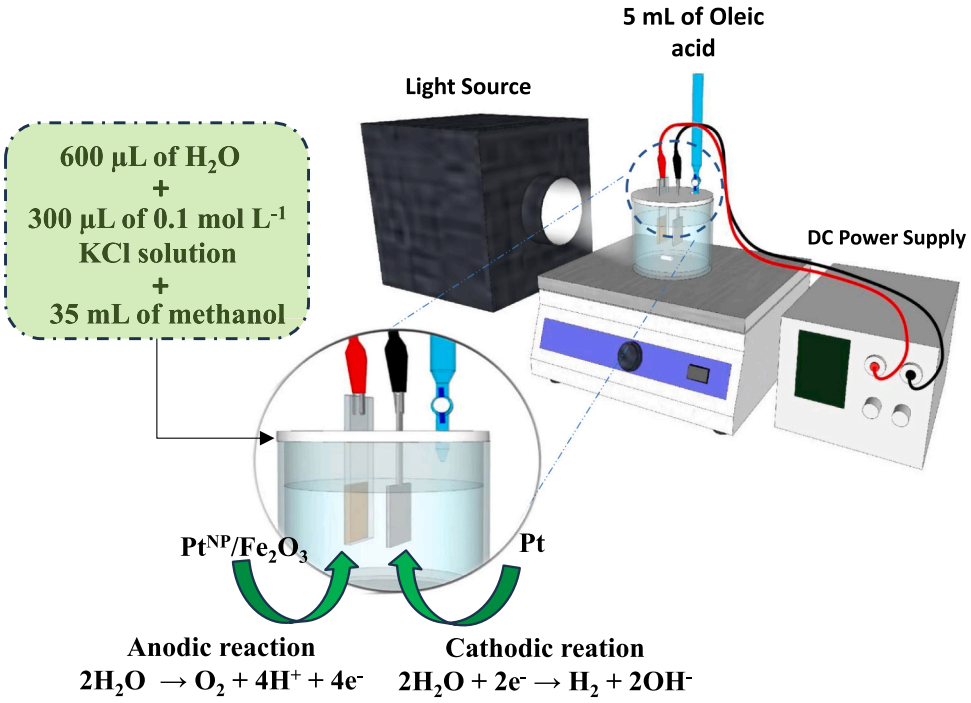

Fig. 2. Schematic representation of electrochemical cell used to produce biodiesel.

potential to the electrochemical cell, Longwei DC Power Supply equipment with programmable output of up to 5 A/32 V was used. In the positive pole of the DC Source was connected the hematite film (α-Fe_2O_3), while in the negative pole was connected a platinum (Pt) foil with approximately 3.0 cm^2. To evaluate the effect of electrode polarization on pH variation in the electrochemical cell, before the oleic acid addition, a glass electrode of the pH meter was immersed in the biodiesel precursor solution formed by 35 mL of methanol, 600 μL of deionized water and 300 μL of 0.1 mol L^{-1} KCl solution, as supporting electrolyte. Different potentials were applied, and the pH variation was recorded. For the synthesis of biodiesel, 5 mL of oleic acid (from Dinamica P.S.) was placed in a burette and positioned in the electrochemical cell according to the scheme shown in Fig. 2. After polarization of the electrodes at 30 V and irradiation with polychromatic light, the acid was dripped into the reaction system at a speed of 1 mL min^{-1}.

2.5. Products analysis

After the electrochemical reaction, the products obtained were initially investigated by Thermogravimetric analysis (TGA) in a Shimadzu Model TGA-50 thermobalance equipment. The TGA curves were registered using an air atmosphere with a flow of 80 mL/min, a heating rate of 10 °C/min, with a temperature range from 25 to 600°C. Also, analysis by gas chromatography coupled to mass spectrometry (GC-MS) of the reaction product was carried out on a gas chromatograph GCMS-QP2010 SE Ultra (Shimadzu) coupled to a mass spectrometer, equipped with an AOC-5000 autosampler and DB capillary column-5MS IU ((5 %-phenyl)-methylpolysiloxane, 30 m x 0.25 mm×0.25 μm). For analysis, a 1 μL aliquot of the sample (0.5 mg mL^{-1} in AcOEt) was injected in split mode (50:1), an injector temperature of 300°C, and an interface temperature of 310 °C. The oven programming was of initial temperature of 70 °C maintained for 2 min, a heating rate of 6°C min^{-1} to 310 °C, kept for 20 min. The total analysis time was 62 min. The carrier gas was helium (99.9999 %; White Martins) with a constant flow of 1 mL min^{-1} and solvent cutting time of 4 min. The mass spectrometer with quadrupole analyzer, ion source temperature of 260°C, electron ionization at 70 eV and mass range of 45–650 Da. The identification was carried out based on the fragmentation patterns and molecular masses expected for the usual methyl esters and comparison with software libraries (Wiley 229 and NIST 08).

3. Results and discussion

3.1. Structural, morphological, and optical characterization of the films

To investigate the structure of the sample, the calcined films were analyzed by X-ray diffraction (XRD) technique. XRD patterns recorded for FTO-glass substrate, α-Fe_2O_3, and Pt^{NP}/α-Fe_2O_3 samples are shown in Fig. 3. The registered diffractograms are compared with information from the *Inorganic Crystal Structure Database* (ICSD). From Fig. 3 it is possible to see that both films present intense signals at 2θ equal to 26.5°, 33.7°, 37.6°, 51.5°, 54.5°, 61.5° and 65.5° attributed to the SnO_2 of a glass-FTO conductive substrate (FTO-glass). Other diffraction signals agree with ICSD Card number #7799. These signals were indexed to the crystallographic planes (012), (104), (110), (112), (202), (114), (203), (024), (190) and (030), characteristic of the trigonal structure of α-Fe_2O_3 phase, with a spatial symmetry group ($R\bar{3}c$) [17]. The average crystallite size (D) for the α-Fe_2O_3 and Pt^{NP}/α-Fe_2O_3 samples was calculated from the Debye-Scherrer equation, as shown in Eq. 3[29].

$$D = \frac{K\lambda}{\beta Cos\theta} \quad (3)$$

where K is the Scherrer constant, which represents the form factor ($K = 0.9$), λ is wavelength used in the analysis (0.154184 nm), β is the Full width at half maximum (FWHM) of the peak, and θ is the diffraction angle.

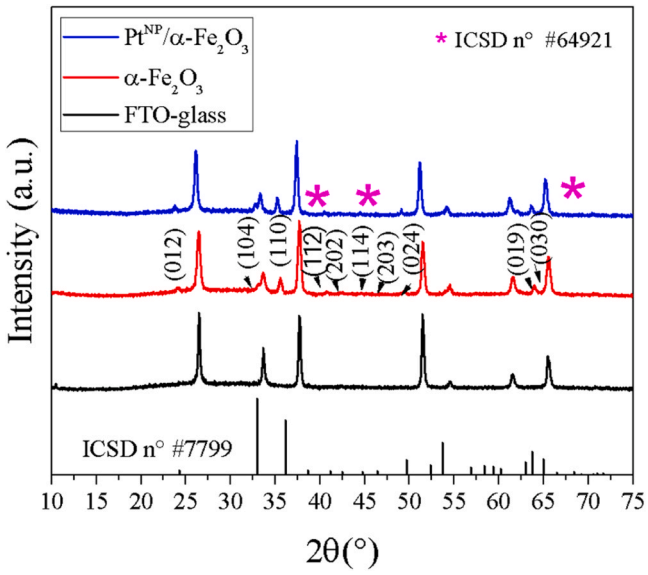

Fig. 3. XRD pattern of FTO-glass, α-Fe_2O_3, and Pt^{NP}/ α-Fe_2O_3 films thermally treated at 500°C for 2 h. The vertical lines indicate the positions of the planes and intensities of the FTO-glass and films.

The average crystallite size showed results very similar, which were estimated at 22±3 and 21±5 nm for α-Fe_2O_3 and Pt^{NP}/α-Fe_2O_3 samples, respectively. The diffraction signals for the PtNP/α-Fe_2O_3 film did not show diffraction signals of sufficient intensity to identify the metallic Pt nanoparticles. However, the expected 2theta values for the diffraction signals of metallic Pt are identified with an asterisk symbol (*) in Fig. 3, according to ICSD card number #243678 [18,19].

The porous morphology of the electrodes also directly influences the catalytic performance of the materials used as films. In this way, morphological characterization of the films was also carried out using FEG-SEM. FEG-SEM images with 200k magnification are shown in Fig. 4. It is possible to observe that both electrodes present a morphology that resembles nanorods, which corroborates previous studies by our research group [17]. As can be seen in Fig. 4a-b, Pt^{NP} deposited on hematite does not change the shape of the nanorods. From the mapping using energy-dispersive X-rays (EDS), it is possible to notice the presence and distribution of the elements that make up the surface of each sample. Fig. 4c-d shows the distribution of elements for the α-Fe_2O_3 and Pt^{NP}/α-Fe_2O_3 samples, respectively. From the EDS analysis, a homogeneous distribution of elements in the samples is observed. In addition, from the FEG-SEM image in Fig. 4b, it is not possible to observe the Pt^{NPs} existence. However, the EDS analysis revealed the presence of Pt with good distribution in the Pt^{NP}/α-Fe_2O_3 sample.

Based on ultraviolet-visible spectroscopy (UV-Vis), it was possible to optically characterize the prepared films. Fig. 5 shows the transmittance values as a function of wavelength (λ) for each sample. As can be seen in the UV-Vis curves, there is an abrupt reduction in the transmittance of both films at $\lambda < 600$ nm, which is attributed to electron transition from the valence band (VB) to the conduction band (CB), overcoming the E_{bg} [30] However, the transmittance is lower for the Pt^{NP}/α-Fe_2O_3 film, indicating that the Pt nanoparticles increase radiation absorption.

Based on the data obtained by UV-Vis spectroscopy, it was possible to estimate the value of the E_{bg} of the films, using the Wood-Tauc method [27]. The curves inset in Fig. 5 show the E_{bg} values were approximately 2.1 eV for both samples, indicating that the surface modification with Pt^{NP} does not change the structure of the material, i.e., there is no material doping [18,29].

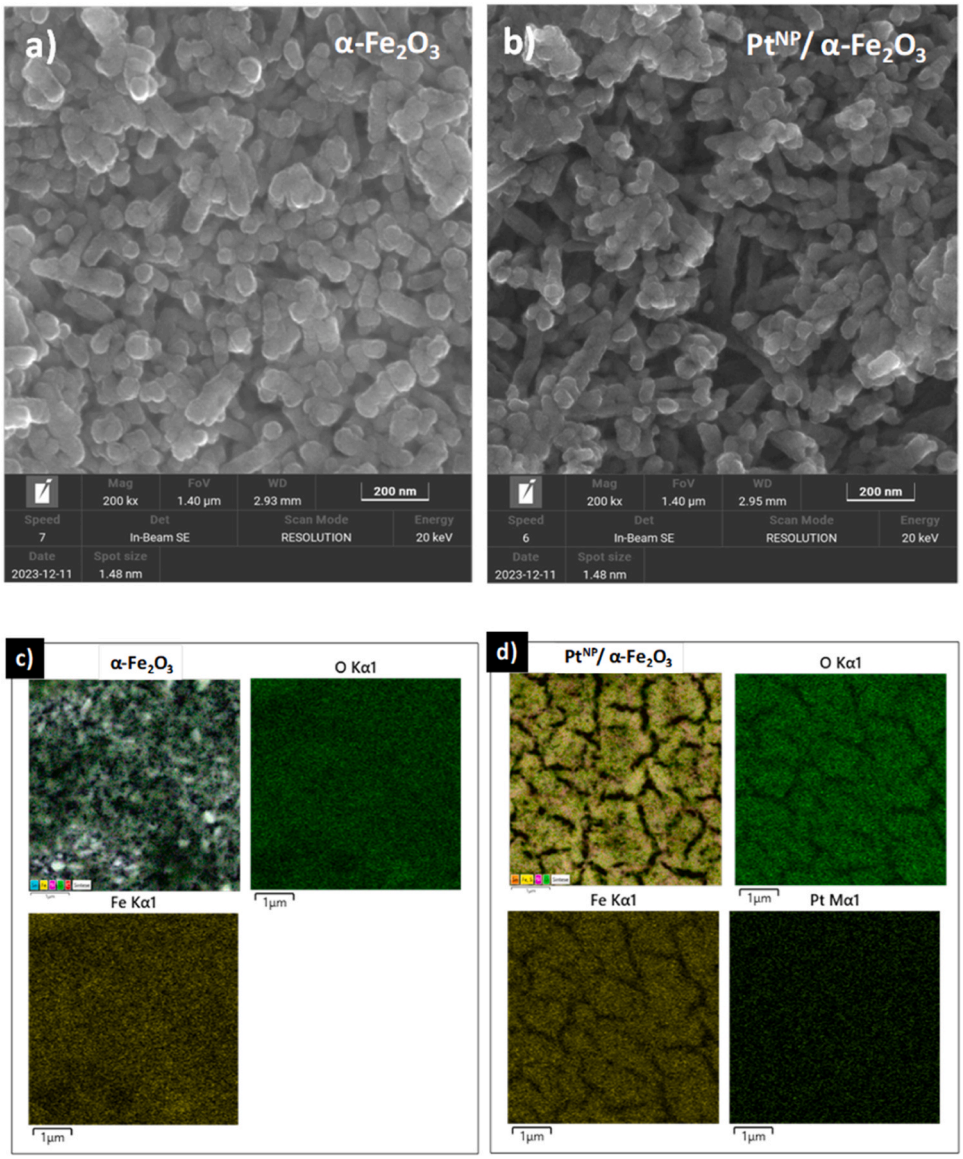

Fig. 4. (a-b) FEG-SEM images and (c-d) EDS mapping with element distribution for the α-Fe_2O_3 and Pt^{NP}/α-Fe_2O_3 samples, respectively.

3.2. Photoelectrochemical characterization of the films

Electrochemical measurements of the α-Fe_2O_3 and Pt^{NP}/α-Fe_2O_3 films were performed using an electrochemical cell with a capacity of 15 mL, in a solution of Na_2SO_4 0.1 mol L^{-1} as a supporting electrolyte. The open circuit potential (V_{OC}) of the films was recorded under irradiation and dark conditions. Both samples showed negative photopotential, which represents the difference between the potential obtained for the system under light conditions and in the dark. The α-Fe_2O_3 and Pt^{NP}/α-Fe_2O_3 displayed a ΔV_{OC} of −80 mV, and −0.50 mV, respectively. The negative ΔV_{OC} values of the films confirm that the materials are n-type semiconductors, suitable for photo-oxidation processes [30–32].

Considering that films are photoanode, i.e., n-type semiconductors, Linear Scanning Voltammetry (LSV) was performed in anodic potential direction, from −0,01 to 0.8 V (*vs* Ag/AgCl). Fig. 6a shows LSV curves registered with a light interruption (chopper) of 0.2 Hz and a scan rate of 2 mV s^{-1}. The Pt^{NP}/α-Fe_2O_3 film displayed a photocurrent of 4.9 µA cm^{-2}, whereas the α-Fe_2O_3 film presented a photocurrent of 1.4 µA cm^{-2}. According to the semiconductors band theory, the electrons are excited from the VB to CB, forming an electron-hole pair. However, the electron-hole recombination can occur, when the electrons return to the VB [33,34]. To reduce recombination, metallic nanoparticles are added to the films. Nanoparticles such as Pt act as electron "traps", scattering or absorbing light, thus delaying charge recombination and increasing the photocurrent of the films [35,36]. So, the superior photocurrent for the Pt^{NP}/α-Fe_2O_3 sample can be associated with the effect of traps created by Pt^{NP}.

From LSV registered with light interruption, it was possible to determine the flat band potential (E_{fb}) of the semiconductor by the Butler-Gärtner model. This methodology is based on the extrapolation of linearization of square photocurrent in the function of potential, according to Eq. 4.

$$Iph = \alpha W0q\varphi0\sqrt{(E - E_{fb})} \quad (4)$$

where α is the absorption coefficient, W_0 is the depletion layer, φ0 is the photon flux, q is the electron charge, and E_{fb} is the flat band energy. Based on the experimental data, it was possible to calculate the E_{fb} for the α-Fe_2O_3 and Pt^{NP}/α-Fe_2O_3 samples at −0.050 and 0.001 V (*vs* Ag/AgCl), respectively. Fig. 6b presents the curves obtained based on the Butler-Gärtner model. Fig. 6c shows the relative positions of the BV and

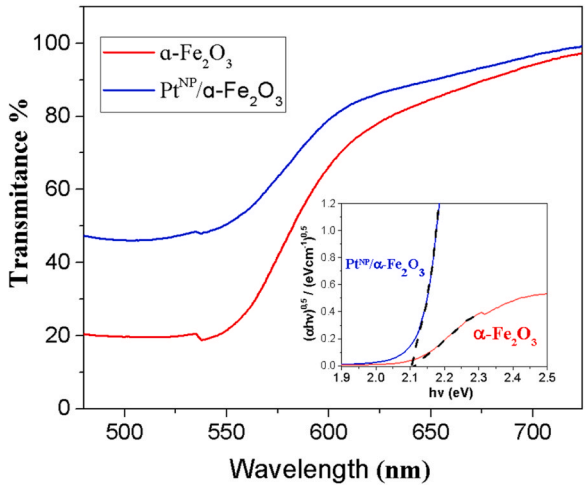

Fig. 5. UV-Vis curves in transmittance mode for α-Fe_2O_3 films (red line) and Pt^{NP}/α-Fe_2O_3 (blue line) calcined at 500°C for 2 h. Inset: band gap energy estimated by the Wood-Tauc methodology considering indirect transition energy.

CB edge potentials for the electrodes considering the pH of 5.8 of the electrochemical system. Based on previous studies, the flat band potentials of the electrodes are suitable for reactive oxygen species (ROS) formation from the water photoelectrolysis, confirming their suitable applications as photoanodes [31,32,37].

3.3. pH test with the biodiesel precursor solution and mechanism of biodiesel production

As discussed, esterification via the electrochemical route is catalyzed by the hydroxyl ion (OH^-) formed at the cathode. Subsequently, OH^- reacts with alcohol (R–OH) producing R–O^- species (alkoxy), which are extremely nucleophilic and can react with the carbonyl bonds present in the fatty acid. When the alcohol is methanol (R = H_3C), the product of this reaction is fatty acid methyl esters (FAME), which can be classified as biodiesel [38–40]. Thus, the catalysis process of biodiesel formation is initiated by the formation of OH^- in the reaction medium. Fig. 7 show curves of pH in function of voltage application in electrochemical cells. This study was conducted with the electrochemical system under polarization conditions and a pH meter electrode immersed into the solution, as described in Section 2.4.

The hematite film is a suitable photoanode, that is, capable of oxidizing water molecules and other species present in the electrolyte while providing electrons to the cathode of the electrochemical cell. From Fig. 7 it is possible to see that the pH changes to higher values (alkaline), according to the increase in potential. Thus, it is possible to state that OH^- is formed on the cathode surface from the reduction reaction of water molecules, while species are oxidized on the anode surface. Furthermore, according to Fig. 7, pH 14 is more easily reached when the Pt^{NP}/α-Fe_2O_3 electrode is utilized. From Fig. 7 hematite modified with Pt^{NP} presents a better charge transfer than the pure Pt electrode.

In an early study, we discussed that α-Fe_2O_3 presents greater interaction with water molecules, reducing the overpotential for RDO [17]. Furthermore, we have two additional contributions that can corroborate to the superior catalytic effect of the reaction system: (i) the photooxidation reactions occurring at the anode can serve as additional sources of electrons for the cathode, and (ii) Pt^{NP} can act as co-catalysts and prevent the charge recombination process in the semiconductor. A previous study discusses that the chloride ions added as electrolytic support must be oxidized before oxidation of the methanol that is in excess in the precursor solution occurs, due to its low standard oxidation potential (-1.36 V vs. RHE) [41]. However, considering the ROS formation process, discussed previously, excess methanol should also contribute as a source of electrons for the electrochemical synthesis of biodiesel when the hematite electrode is used as a photoanode. Thus, the chemical equations presented from 5 to 10 can summarize the charge

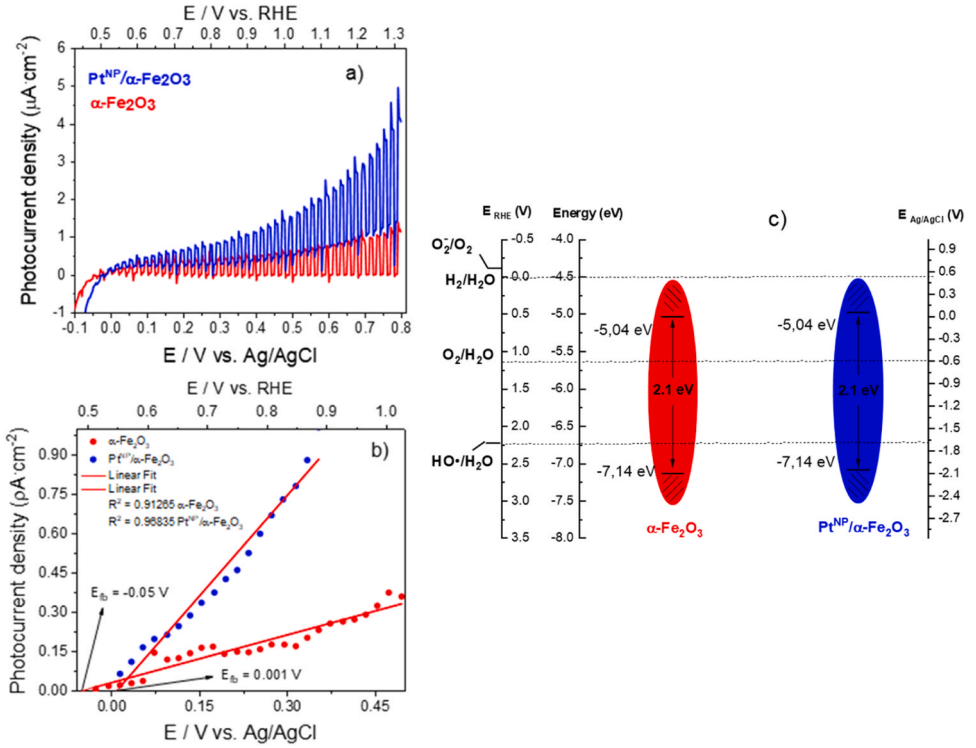

Fig. 6. Linear Scanning Voltammetry registered under interruption of light registered in scan rate of 2 mV s^{-1} for (a) α-Fe_2O_3 and Pt^{NP}/α-Fe_2O_3 samples. Curves of $(I_{ph})^2$ vs. the applied potential for E_{fb} for (b) α-Fe_2O_3 and (c) Pt^{NP}/ α-Fe_2O_3 samples, based on the Butler-Gärtner model.

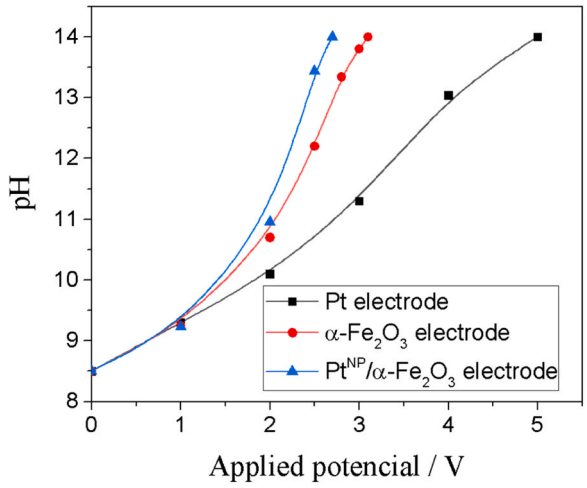

Fig. 7. pH variation study for the photoelectrochemical system under polarization variation and different electrodes.

transfer steps and the formation of chemical species until the biodiesel.

Anodic reaction:

$$2Cl^- \rightarrow Cl_2 + 2e^- \quad (5)$$

$$H_3COH + H_2O \rightarrow CO_2 + 6H^+ + 6e^- \quad (6)$$

Cathodic reaction:

$$2H_2O + 2e^- \rightarrow H_2 + 2OH^- \quad (7)$$

$$2H^+ + 2e^- \rightarrow H_2 \quad (8)$$

Proton transfer reaction:

$$CH_3OH + OH^- \rightarrow CH_3O^- + H_2O \quad (9)$$

Esterification reaction:

$$R_1\text{–}COOH + CH_3O^- \rightleftharpoons R_1\text{–}COO\text{–}CH_3(\text{biodiesel}) + H_2O \quad (10)$$

As discussed before and according to Moradi et al. [42], the hydroxyl formed at the cathode must react with methanol to produce methoxy, which is highly reactive and acts as a nucleophile. After the formation of methoxy, a nucleophilic attack occurs on the carbonyl of the fatty acid, which forms a carbocation, then an intermediate is formed. Then, a rearrangement of the molecule must occur to form the FAME, as shown in Fig. 8.

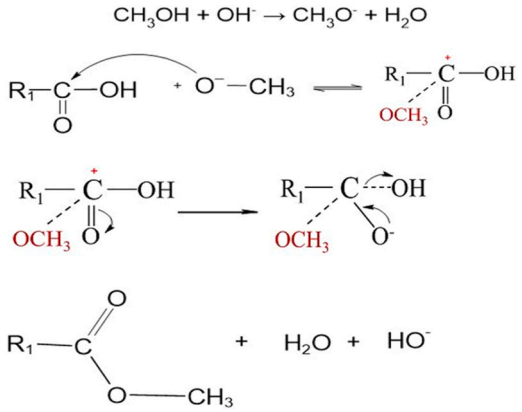

Fig. 8. Mechanism of biodiesel production by esterification.

3.4. Characterizations of the products formed after the catalytic process

3.4.1. Thermogravimetric analysis (TGA)

Initially, the products obtained after photoelectrocatalytic reaction were analyzed by thermogravimetric analysis (TGA) and compared with the TGA curve obtained for oleic acid. Previous studies by Chand et al. [43] demonstrated that TGA curves can provide qualitative and quantitative information for evaluating biodiesel. Thermogravimetric curves for oleic acid and biodiesel prepared by electrochemical synthesis are shown in Fig. 9. The thermal stability evaluation of biodiesel by thermogravimetric analysis becomes very important for understanding the chemical reactivity of fatty acids and their esters. Changes in the profile of the TGA curves can be used as initial information to verify the conversion of precursors into biodiesel [44]. Changes in mass percentage occurred from the formation and breaking of physical and chemical bonds at elevated temperatures [43,45].

Fig. 9 shows that the sample prepared by electrochemical synthesis displayed greater mass loss than oleic acid, in the same temperature range (33–220°C). According to the TGA curves, the thermal decomposition temperature of oleic acid is higher than that of the electrochemical catalysis product, which suggests that the formation of FAME may have occurred. The first derivate of the weight (dashed curves) presented a displacement in thermal decomposition for biodiesel and oleic acid, which occurred at 270 and 288 °C, respectively. This is due to the higher viscosity and bond strengths of the fatty acid in comparison to biodiesel. Thus, the TG curves of the samples can be used to indicate the conversion of oleic acid into biodiesel [46].

3.4.2. Gas chromatography coupled to mass spectrometry (CG-MS)

GC-MS was used to investigate the product of electrochemical catalysis. Fig. 10a shows the chromatograms of the FAMEs obtained by photoelectrochemical synthesis. The mass spectrum for signal (5) of the chromatogram is shown in Fig. 10b. Considering the mass of the fragments (m/z) obtained, the signal (5) was attributed to Methyl 9-octadecenoate. Based on the GC-MS results, it was possible to confirm the esterification of oleic acid into methyl 9,12-octadecadienoate (0.78 %), methyl 9-octadecenoate (5.76 %). The Table 1 shows the type and percentage of fatty acid methyl esters obtained from photoelectrochemical route.

The GC-MS analysis revealed that the photoelectrochemical route was responsible for conversing around 7 % of the oleic acid in FAMEs, within a 2 h reaction time. Considering that oleic acid is the majority compound of the starting reagent, the main methyl ester obtained was methyl 9-octadecenoate. The other methyl esters obtained in smaller proportions can be attributed to the presence of other fatty acids present

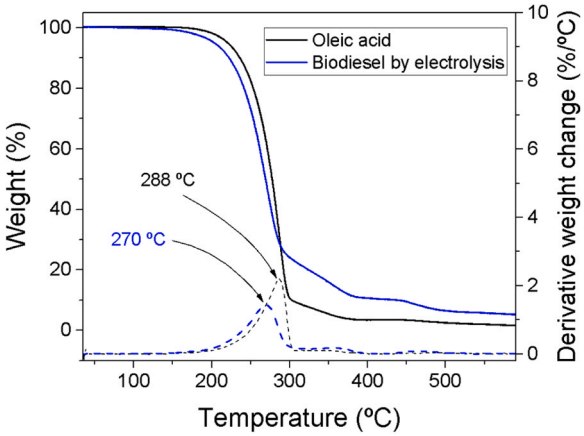

Fig. 9. Comparison of TGA curves recorded for oleic acid used as precursor reagent and product obtained after the photoelectrochemical reaction to prepare biodiesel.

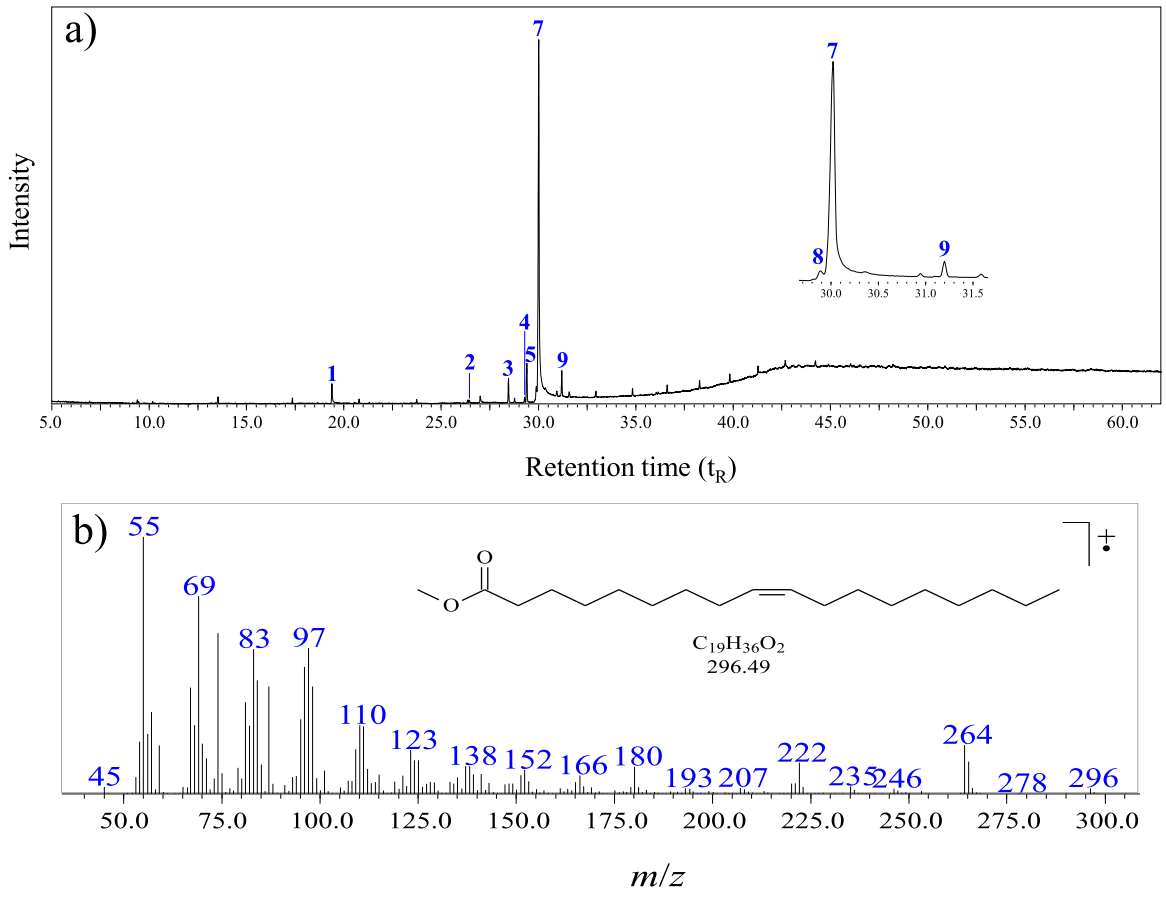

Fig. 10. Gas chromatography coupled to mass spectrometry of the electrochemical synthesis of biodiesel.

Table 1
FAMEs identified in the sample prepared by photoelectrochemical route from oleic acid.

Signal	Compound	Area (%)	t_R (min)	Fragments [*m/z* (%)]
1	Dodecanoic acid	2.84	19.391	73 (100); 60 (89); 57 (48); 55 (45); 129 (34); 200 ($M^{+\bullet}$ 4)
2	Methyl hexadecanoate	0.36	26.455	74 (100); 87 (70); 75 (22); 55 (22); 143 (20); 270 ($M^{+\bullet}$ 4)
3	Hexadecanoic acid-TMS	3.18	28.464	117 (100); 73 (86); 75 (62); 313 (54); 129 (37); 328 ($M^{+\bullet}$ 2)
4	Methyl 9,12-octadecadienoate	0.78	29.290	67 (100); 81 (80); 95 (57); 55 (50); 58 (48); 294 ($M^{+\bullet}$ <1)
5	Methyl 9-octadecenoate	5.76	29.403	55 (100); 69 (77); 74 (59); 83 (58); 296 ($M^{+\bullet}$ 2)
6	9,12-octadecadienoic acid	1.53	29.887	67 (100); 81 (82); 95 (58); 68 (54); 82 (54); 280 ($M^{+\bullet}$ 5)
7	9-octadecenoic acid	81.15	30.020	55 (100); 69 (85); 83 (65); 97 (58); 57 (41); 282 ($M^{+\bullet}$ 1)
8	9-octadecenoic acid-TMS	3.49	31.199	73 (100); 117 (95); 75 (84); 129 (67); 55 (55); 339 (47); 354 ($M^{+\bullet}$ 3)
9	Octadecanoic acid-TMS	0.91	31.586	117 (100); 73 (73); 341 (65); 75 (53); 132 (43); 129 (43); 356 ($M^{+\bullet}$ 4)

in the starting reagent. Even though, the reaction did not convert all initial reagents into FAMEs, the studies presented here demonstrate that the photoelectrocatalytic route for preparing biodiesel is promising, considering there was no soap formation as an undesirable product. Furthermore, as the catalyst reactant is formed on the α-Fe_2O_3 electrode, an extra step to separate the catalyst from the reaction medium is not necessary.

For comparison purposes, biodiesel was prepared by conventional route, from esterification by homogeneous catalysis. The reaction product was evaluated by GC-MS and the data is presented in the Supporting Information, in Fig. 1S and Table 1S. From Fig. 1S it is possible to see that the product of the conventional route reaction produced a chromatogram with 6 signals, with peak (4) being the most intense. Table 1S shows the methyl esters obtained by the conventional route and the percentage of each of them. In this case, the reaction had a yield of 100 % conversion of the starting reagent into FAMEs, with a higher percentage for 9Z-Octadec-9-methyl enoate, which reached almost 84 %.

Other studies have been carried out aiming at the electrochemical preparation of biodiesel, with a higher yield of FAMEs. However, these studies have been carried out with the presence of strong bases such as KOH or NaOH as supporting electrolyte [8,15,47]. The presence of these reagents seems to contradict the main justification for using the electrochemical route, which would be the formation of OH- groups from the electrolysis of water. Thus, the study proposed here presents a route free of co-solvent and alkaline reagent. Therefore, the application of the methodology base on hematite electrode as photoanode for biodiesel production proved to be promising for this field of study.

4. Conclusions

Hematite film electrodes with nanoparticles (Pt^{NP}/α-Fe_2O_3) were produced, as well as the functionalization process of films with Pt^0 nanoparticles. The bandgap energy (E_{BG}) of the α-Fe_2O_3 and Pt^{NP}/α-Fe_2O_3 films was approximately 2.1 eV, for both samples. Electrochemical measurements showed that the semiconductors are of n-type

material, that is, photoanode. Biodiesel synthesis was carried out under different conditions. In addition to the electrochemical route, biodiesel was synthesized by a conventional method. The products obtained were analyzed by thermogravimetry (TGA) and gas chromatography coupled to mass spectrometry (GC-MS). The electrochemical synthesis showed a curve below the oleic acid decomposition temperature. This suggests there was a change in the composition of oleic acid, which led to a lower initial decomposition temperature. In addition to thermogravimetric analysis, the products were analyzed by gas chromatography. Based on the results obtained from GC-MS, it was possible to confirm the esterification of oleic acid in the FAMEs such as methyl 9-octadecenoate, methyl hexadecanoate, and methyl hexadecanoate. Based on what was discussed, it can be confirmed that hematite electrodes decorated with Pt nanoparticles can synthesize biodiesel through the esterification of oleic acid. Thus, the application of this photoelectrocatalytic route for biodiesel production proved to be promising for this field of study.

CRediT authorship contribution statement

Geraldo E. Luz-Jr: Writing – original draft, Methodology, Conceptualization. **Reginaldo S. Santos:** Writing – review & editing, Supervision, Project administration, Methodology, Conceptualization. **Rejane M.P. Silva:** Resources, Methodology, Investigation. **Sidney G. Lima:** Formal analysis, Data curation. **Tiago P. Braga:** Visualization, Investigation, Formal analysis. **Isolda Costa:** Validation, Investigation, Formal analysis. **Wagner N. Soares:** Writing – original draft, Methodology, Investigation, Data curation, Conceptualization. **Antonio G.R. Costa:** Methodology, Investigation, Formal analysis.

Declaration of Competing Interest

The authors declare that they have no known competing financial interests or personal relationships that could have appeared to influence the work reported in this paper.

Data availability

No data was used for the research described in the article.

Acknowledgments

The authors would like to thank the research funding agencies FAPEMA (Process number BM-02233/21), CAPES (88887.931740/2024–00 and 88881.691127/2022-01) and CNPq (Process number 310720/2023–0) for scholarships granted to research participants and other financial support.

Appendix A. Supporting information

Supplementary data associated with this article can be found in the online version at doi:10.1016/j.cattod.2024.114997.

References

[1] M. Guo, W. Jiang, J. Ding, J. Lu, Highly active and recyclable CuO/ZnO as photocatalyst for transesterification of waste cooking oil to biodiesel and the kinetics, Fuel vol. 315 (May 2022) 123254, https://doi.org/10.1016/j.fuel.2022.123254.

[2] B.H.H. Goh, et al., Progress in utilisation of waste cooking oil for sustainable biodiesel and biojet fuel production, Energy Convers. Manag vol. 223 (Nov. 2020) 113296, https://doi.org/10.1016/j.enconman.2020.113296.

[3] D. Neupane, Biofuels from renewable sources, a potential option for biodiesel production, Bioengineering vol. 10 (1) (Dec. 2022) 29, https://doi.org/10.3390/bioengineering10010029.

[4] M. Abdollahi Asl, K. Tahvildari, T. Bigdeli, Eco-friendly synthesis of biodiesel from WCO by using electrolysis technique with graphite electrodes, Fuel vol. 270 (Jun. 2020) 117582, https://doi.org/10.1016/j.fuel.2020.117582.

[5] W.P. Wicaksono, S.A. Jati, I. Yanti, P.K. Jiwanti, Co-solvent free electrochemical synthesis of biodiesel using graphite electrode and waste concrete heterogeneous catalyst: optimization of biodiesel yield, Bull. Chem. React. Eng. Catal. vol. 16 (1) (Mar. 2021) 179–187, https://doi.org/10.9767/bcrec.16.1.10310.179-187.

[6] D.Y.C. Leung, X. Wu, M.K.H. Leung, A review on biodiesel production using catalyzed transesterification, Appl. Energy vol. 87 (4) (Apr. 2010) 1083–1095, https://doi.org/10.1016/j.apenergy.2009.10.006.

[7] H. Taher, S. Al-Zuhair, A.H. Al-Marzouqi, Y. Haik, M.M. Farid, A review of enzymatic transesterification of microalgal oil-based biodiesel using supercritical technology, Enzym. Res vol. 2011 (Sep. 2011) 1–25, https://doi.org/10.4061/2011/468292.

[8] N. Singh, et al., Progress and facts on biodiesel generations, production methods, influencing factors, and reactors: A comprehensive review from 2000 to 2023, Energy Convers. Manag vol. 302 (Feb. 2024) 118157, https://doi.org/10.1016/j.enconman.2024.118157.

[9] S.M. Farouk, A.M. Tayeb, S.M.S. Abdel-Hamid, R.M. Osman, Recent advances in transesterification for sustainable biodiesel production, challenges, and prospects: a comprehensive review, Environ. Sci. Pollut. Res. vol. 31 (9) (Jan. 2024) 12722–12747, https://doi.org/10.1007/s11356-024-32027-4.

[10] A.S. Elgharbawy, Wagih A. Sadik, O.M. Sadek, M.A. Kasaby, A review on biodiesel feedstocks and production technologies, J. Chil. Chem. Soc. vol. 66 (1) (Jan. 2021) 5098–5109, https://doi.org/10.4067/S0717-97072021000105098.

[11] G. Guan, K. Kusakabe, Synthesis of biodiesel fuel using an electrolysis method, Chem. Eng. J. vol. 153 (1–3) (Nov. 2009) 159–163, https://doi.org/10.1016/j.cej.2009.06.005.

[12] K. Sipa, M. Brycht, S. Skrzypek, The effect of the supporting electrolyte on the voltammetric determination of the veterinary drug nitroxinil, J. Electroanal. Chem. vol. 827 (Oct. 2018) 21–26, https://doi.org/10.1016/j.jelechem.2018.09.006.

[13] H. Dotan, et al., Decoupled hydrogen and oxygen evolution by a two-step electrochemical–chemical cycle for efficient overall water splitting, Nat. Energy vol. 4 (9) (Sep. 2019) 786–795, https://doi.org/10.1038/s41560-019-0462-7.

[14] M. Darwin, M. Thifal, Z. Alwi, A.Pratama Murizal, M. Rizal, The synthesis of biodiesel from palm oil and waste cooking oil via electrolysis by various electrodes, Case Stud. Chem. Environ. Eng. vol. 8 (Dec. 2023) 100512, https://doi.org/10.1016/j.cscee.2023.100512.

[15] V. Aslan, T. Eryilmaz, Polynomial regression method for optimization of biodiesel production from black mustard (Brassica nigra L.) seed oil using methanol, ethanol, NaOH, and KOH, Energy vol. 209 (Oct. 2020) 118386, https://doi.org/10.1016/j.energy.2020.118386.

[16] P. Moradi, M. Saidi, A.T. Najafabadi, Biodiesel production via esterification of oleic acid as a representative of free fatty acid using electrolysis technique as a novel approach: non-catalytic and catalytic conversion, Process Saf. Environ. Prot. vol. 147 (Mar. 2021) 684–692, https://doi.org/10.1016/j.psep.2020.12.032.

[17] G.S. Costa, et al., Effect of the applied potential condition on the photocatalytic properties of $Fe_2O_3|WO_3$ heterojunction films,", J. Inorg. Organomet Polym. Mater. vol. 30 (8) (Aug. 2020) 2851–2862, https://doi.org/10.1007/s10904-019-01429-0.

[18] M.J.S. Costa, et al., Investigation of charge recombination lifetime in γ-WO_3 films modified with Ag0 and Pt0 nanoparticles and its influence on photocurrent density, Ion. (Kiel.) vol. 24 (10) (Oct. 2018) 3291–3297, https://doi.org/10.1007/s11581-018-2640-1.

[19] M. JoseitadosSantosCosta, et al., Photocurrent response and progesterone degradation by employing WO_3 films modified with platinum and silver nanoparticles, Chempluschem vol. 83 (12) (Dec. 2018) 1153–1161, https://doi.org/10.1002/cplu.201800534.

[20] M. Mishra, D.-M. Chun, α-Fe_2O_3 as a photocatalytic material: a review, Appl. Catal. A Gen. vol. 498 (Jun. 2015) 126–141, https://doi.org/10.1016/j.apcata.2015.03.023.

[21] H. Dotan, K. Sivula, M. Grätzel, A. Rothschild, S.C. Warren, Probing the photoelectrochemical properties of hematite (α-Fe_2O_3) electrodes using hydrogen peroxide as a hole scavenger, Energy Environ. Sci. vol. 4 (3) (2011) 958–964, https://doi.org/10.1039/C0EE00570C.

[22] Z. Najaf, et al., Recent trends in development of hematite (α-Fe_2O_3) as an efficient photoanode for enhancement of photoelectrochemical hydrogen production by solar water splitting, Int J. Hydrog. Energy vol. 46 (45) (Jul. 2021) 23334–23357, https://doi.org/10.1016/j.ijhydene.2020.07.111.

[23] M. Taleblou, M.F. Camellone, S. Fabris, S. Piccinin, CO oxidation over platinum nanoclusters: unraveling the role of the cluster size and the supporting surface, J. Phys. Chem. C. vol. 127 (43) (Nov. 2023) 21132–21149, https://doi.org/10.1021/acs.jpcc.3c05714.

[24] A.I. Osman, et al., Synthesis of green nanoparticles for energy, biomedical, environmental, agricultural, and food applications: a review, Environ. Chem. Lett. vol. 22 (2) (Apr. 2024) 841–887, https://doi.org/10.1007/s10311-023-01682-3.

[25] M. Safaripour, E. Parandi, B. Aghel, A. Gouran, M. Saidi, H.R. Nodeh, Optimization of the microreactor-intensified transesterification process using silver titanium oxide nanoparticles decorated magnetic graphene oxide nanocatalyst, Process Saf. Environ. Prot. vol. 173 (May 2023) 495–506, https://doi.org/10.1016/j.psep.2023.03.039.

[26] M. Guo, W. Jiang, J. Ding, J. Lu, Highly active and recyclable CuO/ZnO as photocatalyst for transesterification of waste cooking oil to biodiesel and the kinetics, Fuel vol. 315 (May 2022) 123254, https://doi.org/10.1016/j.fuel.2022.123254.

[27] D.L. Wood, J. Tauc, Weak absorption tails in amorphous semiconductors, Phys. Rev. B vol. 5 (8) (Apr. 1972) 3144–3151, https://doi.org/10.1103/PhysRevB.5.3144.

[28] M.J. dos S. Costa, et al., Transition metal tungstates AWO_4 (A^{2+} = Fe, Co, Ni, and Cu) thin films and their photoelectrochemical behavior as photoanode for

photocatalytic applications, J. Appl. Electrochem vol. 53 (7) (Jul. 2023) 1349–1367, https://doi.org/10.1007/s10800-023-01851-w.
[29] J.S. Luis, et al., S-doped ZnO photoelectrode modified with silver and platinum nanoparticles and their photocatalytic activity for progesterone degradation, J. Mol. Struct. vol. 1305 (Jun. 2024) 137764, https://doi.org/10.1016/j.molstruc.2024.137764.
[30] M. Synowiec, D. Zákutná, A. Trenczek-Zajac, M. Radecka, The impact of nanometric Fe_2O_3 on the magnetic, electronic, and photocatalytic behavior of TiO_2@Fe_2O_3 heterostructures, Appl. Surf. Sci. vol. 608 (Jan. 2023) 155186, https://doi.org/10.1016/j.apsusc.2022.155186.
[31] D.R.S. Pitombeira, M.J.S. Costa, R.A. Antunes, R.O. Ferreira, R.M.P. Silva, R. S. Santos, Crystalline S-doped TiO_2 photoanodes from amorphous titanium oxysulfide (TiO_xS_y) for photo-oxidation reactions, Opt. Mater. (Amst.) vol. 142 (Aug. 2023) 114081, https://doi.org/10.1016/j.optmat.2023.114081.
[32] M.L. Barbosa, et al., Anionic and cationic dyes removal by degradation via photoelectrocatalysis using a WO_3/$CuWO_4$ heterojunction film as a photoanode, Nano-Struct. Nano-Objects vol. 35 (Jul. 2023) 100993, https://doi.org/10.1016/j.nanoso.2023.100993.
[33] S.M. Kim, H. Lee, J.Y. Park, Charge transport in metal–oxide interfaces: genesis and detection of hot electron flow and its role in heterogeneous catalysis, Catal. Lett. vol. 145 (1) (Jan. 2015) 299–308, https://doi.org/10.1007/s10562-014-1418-y.
[34] F. Malara, et al., α-Fe_2O_3/NiOOH: an effective heterostructure for photoelectrochemical water oxidation, ACS Catal. vol. 5 (9) (Sep. 2015) 5292–5300, https://doi.org/10.1021/acscatal.5b01045.
[35] M.V. de L. Tinoco, M.B. Costa, L.H. Mascaro, J.F. de Brito, Photoelectrodeposition of Pt nanoparticles on Sb2Se3 photocathodes for enhanced water splitting, Electro Acta vol. 382 (Jun. 2021) 138290, https://doi.org/10.1016/j.electacta.2021.138290.
[36] K.H. Leong, A.A. Aziz, L.C. Sim, P. Saravanan, M. Jang, D. Bahnemann, Mechanistic insights into plasmonic photocatalysts in utilizing visible light, Beilstein J. Nanotechnol. vol. 9 (Feb. 2018) 628–648, https://doi.org/10.3762/bjnano.9.59.
[37] R.Y.N. Reis, et al., Enhanced photoelectrocatalytic performance of ZnO films doped with N_2 by a facile electrochemical method, Surf. Interfaces vol. 21 (Dec. 2020) 100675, https://doi.org/10.1016/j.surfin.2020.100675.
[38] C. Zhang, S.A. Sultan, R. T, X. Chen, Biotechnological applications of S-adenosyl-methionine-dependent methyltransferases for natural products biosynthesis and diversification, Bioresour. Bioprocess vol. 8 (1) (Dec. 2021) 72, https://doi.org/10.1186/s40643-021-00425-y.
[39] Y. Souissi, M. Alouini, W. Mnif, Chemical and biological investigation of organic wastes of frying oils and beef fats: valorization for biodiesel production, J. Chem., Vol. 2018 (2018) 1–9, https://doi.org/10.1155/2018/6248047.
[40] G. Yuan, et al., Electrocatalytic methyl esterification of fatty acid using boron-doped-diamond electrodes, Algal Res vol. 46 (Mar. 2020) 101816, https://doi.org/10.1016/j.algal.2020.101816.
[41] K. Li, Q. Fan, H. Chuai, H. Liu, S. Zhang, X. Ma, Revisiting chlor-alkali electrolyzers: from materials to devices, Trans. Tianjin Univ. vol. 27 (3) (Jun. 2021) 202–216, https://doi.org/10.1007/s12209-021-00285-9.
[42] R. Khoshbin, M. Naeimi, F.M. Alikhani, M.S. Hosseini Hashemi, H. Moradi, Novel approach for synthesis of highly active nanostructured MgO/$ZnAl_2O_4$ catalyst via gel-combustion method used in biofuel production from sunflower oil: effect of mixed fuel, Adv. Powder Technol. vol. 34 (11) (Nov. 2023) 104226, https://doi.org/10.1016/j.apt.2023.104226.
[43] P. Chand, Ch.V. Reddy, J.G. Verkade, T. Wang, D. Grewell, Thermogravimetric quantification of biodiesel produced via alkali catalyzed transesterification of soybean oil, Energy Fuels vol. 23 (2) (Feb. 2009) 989–992, https://doi.org/10.1021/ef800668u.
[44] A.E. Atabani, et al., Integrated valorization of waste cooking oil and spent coffee grounds for biodiesel production: blending with higher alcohols, FT–IR, TGA, DSC and NMR characterizations, Fuel vol. 244 (May 2019) 419–430, https://doi.org/10.1016/j.fuel.2019.01.169.
[45] C.T. Alves, M.A. Peters, J.A. Onwudili, Application of thermogravimetric analysis method for the characterisation of products from triglycerides during biodiesel production, J. Anal. Appl. Pyrolysis vol. 168 (Nov. 2022) 105766, https://doi.org/10.1016/j.jaap.2022.105766.
[46] V. Atgur, et al., Essence of thermal analysis to assess biodiesel combustion performance, Energy vol. 15 (18) (Sep. 2022) 6622, https://doi.org/10.3390/en15186622.
[47] G. Yuan, et al., Electrocatalytic methyl esterification of fatty acid using boron-doped-diamond electrodes, Algal Res vol. 46 (Mar. 2020) 101816, https://doi.org/10.1016/j.algal.2020.101816.